Formation of relocatable umbilical defects in a liquid crystal with positive dielectric anisotropy induced via photovoltaic fields

Formation of relocatable umbilical defects in a liquid crystal with positive dielectric anisotropy induced via photovoltaic fields

S. L. Schafforz [a], G. Nordendorf [a], G. Nava [b], L. Lucchetti [b], A. Lorenz [a,]*

[a] Paderborn University, Department of Chemistry, Warburger Str. 100, 33098 Paderborn, Germany

[b] Dipartimento SIMAU, Università Politecnica delle Marche, Ancona, Italy

Keywords: liquid crystal, $LiNbO_3$, umbilics, defect formation, optical vortices

All optically generated, relocatable umbilic defects in a liquid crystal (LC) with positive dielectric anisotropy are reported. The studied samples are made with a Fe-doped $LiNbO_3$ substrate showing the bulk photovoltaic effect and an ITO coated glass plate as covering substrate. Umbilics are created upon exposure with a focused laser beam: They are induced via photo generated fields at the relocatable exposure beam position. The field distribution of these fields is normal to the sample plane at the exposure spot center and has increasingly high in-plane field components in radial direction: Ideal conditions to induce director reorientations with radial symmetry in a LC with positive dielectric anisotropy. The irradiated regions are studied with polarized probe light revealing the patterns characteristic for umbilic defects and the typical doughnut-shaped intensity distributions expected for optical vortex beams. The experimental findings are compared to calculated transmission profiles. Moreover, a LC with negative dielectric anisotropy was studied in the same type of sample for reference.

* Corresponding author at: Department Chemie, Universität Paderborn, Warburger Str. 100, 33098 Paderborn, Germany.
E-mail address: alexander.lorenz@uni-paderborn.de (A. Lorenz).

1. Introduction

The appearance of umbilical defects, in short umbilics, in liquid crystals with negative dielectric anisotropy was described by Rapini in 1973 [1]. Umbilics have received renewed interest [2–6] in the frame of the controlled generation of optical phase singularities, thanks to their ability to generate optical vortex (OV) beams. In an umbilic, an incident optical beam with circular polarization can be converted to a light beam with a ring-shaped intensity distribution. The general advantages of umbilics for this purpose were comprehensively reviewed [6], recently. It has been shown in several works [7–15] that isolated umbilics can be obtained at a desired position for example by electrode patterning and with a photoactivated interface under DC field. Anyway, creating relocatable umbilics in samples without externally applied electric fields remains a challenge.

Umbilics are nonsingular topological defects, which typically appear in a nematic liquid crystal (LC) with negative dielectric anisotropy $\Delta\varepsilon < 0$, in samples where the molecular alignment of the LC is vertical. The local alignment of the LC is described by the director n, a pseudo vector, which is parallel to the average molecular orientation of elongated, rod-shaped molecules, over a small volume element. A schematic of an umbilic in a slab of LC with vertical director alignment at the surfaces is shown in Fig. 1a. Due to the tilted alignment of the LC director and the rotational symmetry, one could describe an umbilic as a vortex in the fluid LC. As shown in Fig. 1a the director field in an umbilic has rotational symmetry, the local director is perpendicular at the center (near $r = 0$) and the local tilt of the director increases with increasing r.

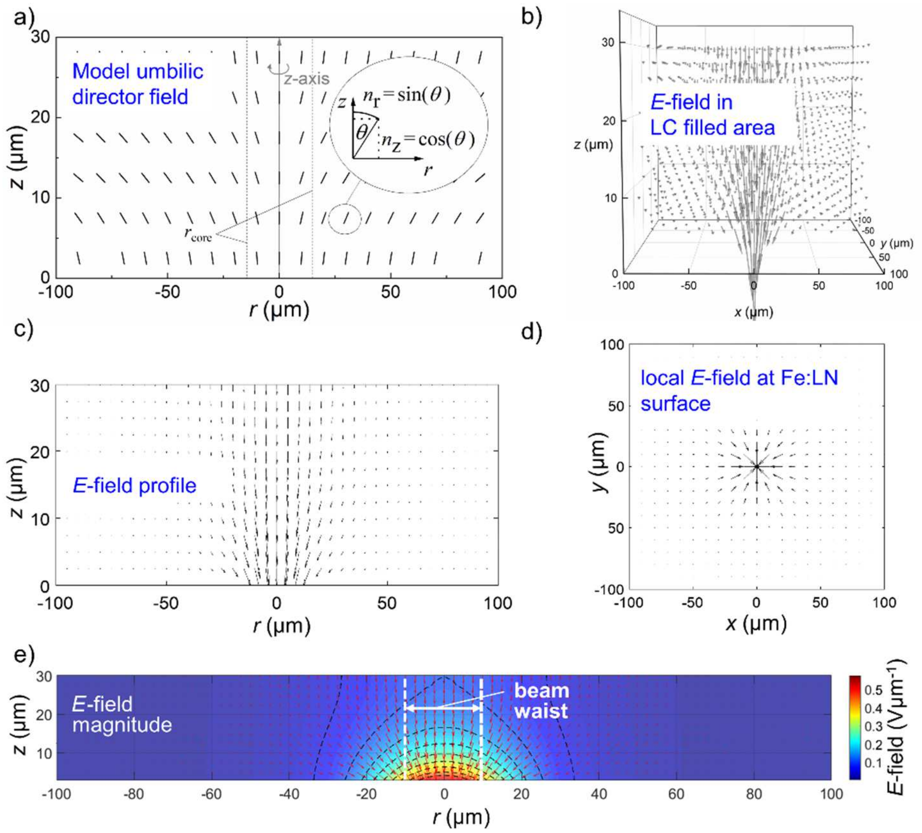

Fig. 1. (a) Director field in a model umbilic. (b) Three-dimensional electric field distribution expected in a sample driven with photovoltaic fields. A value of $\epsilon_{iso} = 7.3$ was used in the LC filled region to calculate the local field distribution. The field distribution was obtained by placing charge distributions on the surfaces of the Fe:LN crystal and applying the image charge method. (c) Profile view of the electric field distribution. (d) Aerial view of the local field distribution at the Fe:LN surface. (e) Magnitude of the field distribution in profile view.

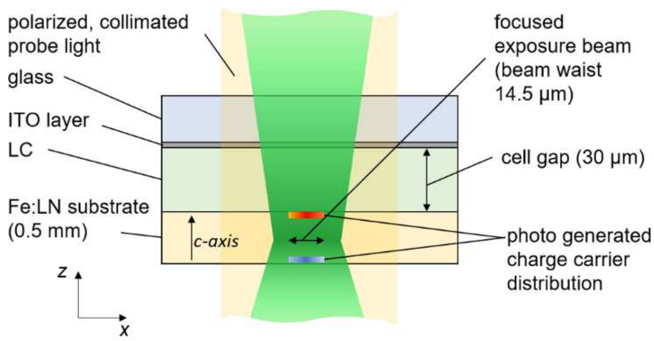

Fig. 2. Schematic of exposed hybridized LC test cell. The samples were investigated with collimated, polarized probe light.

Although they can be created in LCs with negative dielectric anisotropy, umbilics are delicate. According to Meyer [16] two conditions are required at the sample surfaces confining the LC: First, the LC director should be free to reorient in any direction parallel to the substrate surfaces, second, the LC director should be normal to the surfaces of the test cell in the initial state. Therefore, umbilics appear in well-oriented samples of LCs with negative dielectric anisotropy, if an electric field is applied [1,5,6,16,17]. Under these conditions, a reorientation of the LC director is induced without enforcing a preferred direction in the sample plane and the resulting defect is point-like and has well defined rotational symmetry. The external electric field needs to exceed the Fredericks transition threshold (usually ≈ 1 V).

However, this is not the only possible configuration. Here we show that well-defined umbilic defects showing perfect optical texture without pinned, unwanted line defects can be generated in a nematic LC with positive dielectric anisotropy $\Delta\epsilon > 0$ without the need of external electric fields. This is possible in hybridized LC cells, where a field generating *z*-cut Fe doped lithium niobate crystalline (Fe:LN) thin cut was used as one of the cell substrates and the second substrate was a conventional glass plate coated with a conductive ITO layer and treated with lecithin. Upon exposure to light, photovoltaic fields were locally generated within the Fe:LN crystal and confined within the LC layer by the conducting ITO electrode. The photovoltaic field profile in the LC is shown in Fig. 1b–e in the volume, the *rz*-plane, and the *xy*-plane, respectively. Note how the field distribution and the director pattern, both tilted at $|r| > 0$ and vertical at $r \approx 0$, match each other.

A schematic of the exposure setup is shown in Fig. 2. It is worth noting that similar defects in LCs with positive dielectric anisotropy generated without an external electric field have been reported by Brasselet et al. [2,18] in conventional LC cells irradiated by a circularly polarized continuous wave laser beam with beam power > 50 mW, tightly focused to a 2 µm wide focal spot, which could lead to high power densities $> 3 \cdot 10^6\ Wcm^{-2}$ in the focal plane. Here we show that similar defects can be successfully generated in hybrid cells based on a combination of Fe doped lithium niobate (Fe:LN) and LC, using a lower beam power. Our result is a further proof of the versatility of these combined systems and a step forward in the design of novel optofluidic devices with new functionalities.

Crystalline thin cuts of Fe:LN [19–26] have recently been used to address liquid crystal director orientation by means of photovoltaic fields photo-generated via the anomalous photovoltaic effect upon exposure to a low power Gaussian laser beam. As recently shown [27–37], the light induced electric fields were able to penetrate the LC layer and electrically induce reorientation of the LC director, which successfully led to the localized formation and manipulation of topological defects in LC films [34–37]. In samples with a chiral nematic LC [35–37], LC alignment layers were successfully applied to control the interaction with intrinsically formed liquid crystalline defects.

The key point for the light induced formation of umbilics as described here is the spatial profile of the photo generated electric field induced in the LC film by the charge separation generated optically in the Fe:LN substrate. The field distribution shown in Fig. 1b – e was calculated by considering the LC as an isotropic medium and ITO as a perfect conductor. The distribution was obtained by numerically solving the electrostatic problem presented by the samples. Exposure with a focused laser beam induces a charge carrier separation along the crystallographic c-axis (here: parallel to z) in the field generating substrate. As in previous works [32,35–37], this effect was modeled by placing two Gaussian charge carrier distributions $\sigma_{charge} = \pm\sigma_0 e^{-\frac{r^2}{w_{charge}^2}}$ on the top and lower surface of the Fe:LN crystal. A value of w_{charge} = 14 μm was chosen because the Gaussian laser beam used in the exposure experiments had a full width at half maximum of ≈14 μm. In accordance with previously published work [32,35–37] $|\sigma_0|$ was set to 10^4 Cm^{-2}. The dielectric constant of Fe:LN was considered anisotropic ($\epsilon_z = 29$ and $\epsilon_r = 85$) and the thickness of the Fe:LN substrate was set to 500 μm. The ITO layer covering the glass substrate present was treated as a perfect conductor and the image charge method [38] was used to obtain the correct field distribution. A mirror image of the charge distribution of the top Fe:LN surface was placed at a distance of $2 \cdot 30\ \mu m = 60$ μm away from the original top Fe:LN surface. In such a sample, the shape of the field distribution is independent of σ_0. As can be seen in the Figure (Fig. 1b and c), vertical fields locally parallel to the z-direction are present at the center of the exposure spot and fringe fields with high radial components E_r are generated in the area near the exposure spot center. As expected, the fields have rotational symmetry (Fig. 1d).

In a LC with positive sign of $\Delta\varepsilon$, the director tends to realign parallel to the electric field vector. Therefore, the vertical director alignment is expected to be stabilized at the exposure spot center. Since the expected fields have circular symmetry and are decaying with increasing r, in the area nearby the exposure spot center fringe fields should lead to a tilted director realignment with director tilt angle $\theta > 0$.

The all optical generation of umbilic defects in a LC with positive dielectric anisotropy using hybridized cells with a Fe:LN substrate is expected to further expand the applications of these optical singularities, whose primary role in the generation of structured light beams has been recently demonstrated by several studies [4–11,39,40]. Moreover, our results are a further demonstration of the possibilities offered by combined structures based on Fe:LN and LC, whose peculiarity lies in the possibility of using the bulk photovoltaic effect of Fe:LN to obtain an optically induced DC field able to affect the molecular LC director. For completeness, a second LC with negative dielectric anisotropy was studied in the same type of hybridized test cell. An alternative director pattern was preferred in these samples: In contrast to the LC with positive dielectric anisotropy, these defects were obtained at high exposure intensity and exhibited a distorted pattern of director reorientation.

2. Results

2.1. LC with positive dielectric anisotropy

Samples filled with MLC-2087 were first investigated with both crossed and parallel linear polarizers. Polarized optical micrographs were recorded at various exposure intensities and all the experiments were performed at ambient temperature. The typical patterns [5] predicted for umbilic defects with a defect strength of +1 were observed. As described by Pieranski [12], between crossed polarizers, such umbilics cause a pattern of isogyres (usually 4 dark brushes), divided by bright areas, and isochromes: dark, concentric rings. The bright appearance of the areas in-between the isogyres is caused by the locally oblique angle of the optical axis with respect to the polarization direction of the polarizers. The appearance of isochromes is caused by the continuously changing optical phase retardation in radial direction. A pattern of 4 bright areas was indeed seen in the exposed samples at an exposure intensity of 1.42 mW, if investigated with crossed polarizers (Fig. 3a). These bright areas were divided by isogyres, as expected. The absence of isochromes in the pattern can be explained: A schematic of the director field in and near the defect was inserted as red colored lines and wedges. In the initial state, the sample had homeotropic LC alignment and this alignment was maintained in the non-exposed area, which appeared dark, accordingly. The photovoltaic fields led to LC realignment in the exposed area, which in turn led to a locally transmissive, bright state if the local optical axis had an oblique angle with respect to the polarizer orientation. Due to the field profile, the director tilt angle (homeotropic alignment, $\theta = 0°$) was unchanged at the exposure spot center. In radial direction, the effective tilt angle of the director, averaged over the layer thickness, increased, until the maximum tilt angle was reached and then decreased again steadily. As mentioned above, the isolated defect seen was surrounded by non-reoriented ($\theta(r \gg r_{core}) = 0°$) LC and the tilt angle distribution blended into this background continuously. In each of the bright areas, the accumulated optical phase change Γ of the transmitted light travelling within the LC layer reaches values of $\Gamma = \pi$, where locally, maximum values of the transmittance were seen. For the presence of an additional isochrome, the maximum phase change would need to exceed a value of π. For control, the sample was investigated between parallel polarizers, which led toa pattern of 4 dark areas (Fig. 3b), as expected.

In the same samples, patterns with 8 bright (dark) areas were recorded at higher exposure intensity, as shown in Fig. 4a (Fig. 4b). Here, the LC realignment was more pronounced and the induced defects were larger. Therefore, an isochrome was now present (Fig. 4a): As indicated in Fig. 4a, the effective tilt angle of the LC director now reached higher values. The accumulated optical phase change Γ of the transmitted light could reach values of $\Gamma = 2\pi$, the higher variation of the optical phase change led to a dark ring. The patterns shown are characteristic for umbilic defects. If a radial defect leads to such patterns between parallel polarizers, the director field has the correct symmetry of a *q*-plate [6,9,40] with a winding number $q = 1$ and thus, such a director configuration can lead to optical vortex formation.

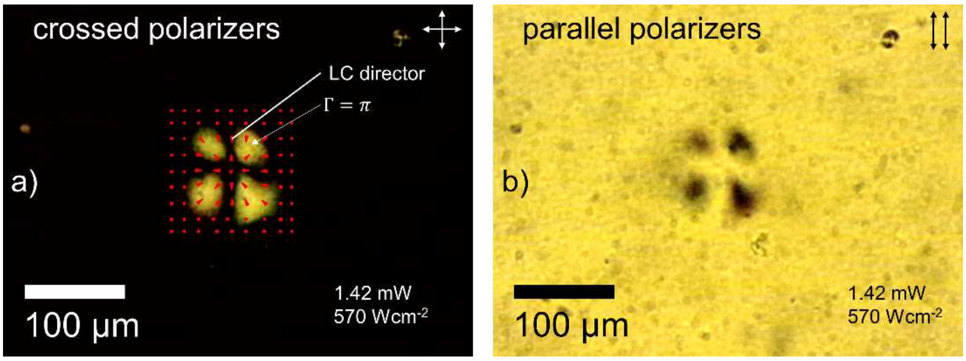

Fig. 3. Polarized optical micrographs of a sample filled with MLC 2087 exposed to a diode laser beam of 1.42 mW overall optical power. The sample was investigated with (a) crossed polarizers, (b) parallel polarizers. A schematic of the LC alignment in and near the locally induced defect was placed in (a). The orientation of the polarizers is indicated with double arrows.

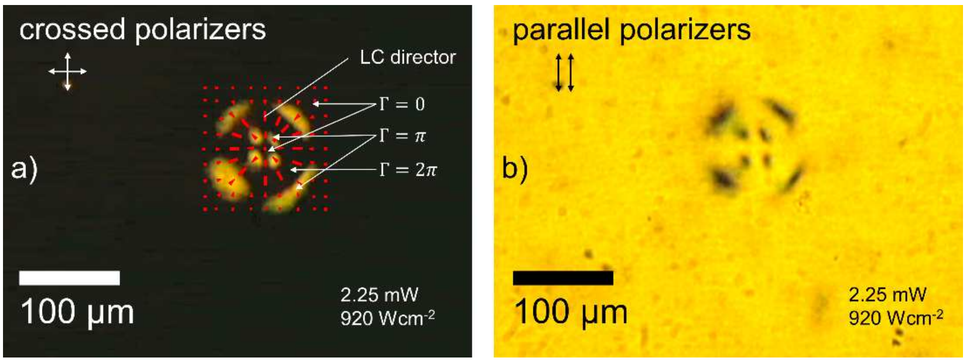

Fig. 4. Polarized optical micrographs of a sample filled with MLC 2087 exposed to a diode laser beam of 2.25 mW overall optical power. The sample was investigated with (a) crossed polarizers, (b) parallel polarizers. A schematic of the LC alignment in and near the locally induced defect was placed in (a). The orientation of the polarizers is indicated with double arrows.

The exposure beam position can be easily relocated in the experiments. An image sequence of the relocation of the exposure beam is shown in Fig. 5. The laser beam was scanned across the sample along the inserted trajectory. The image sequence shown gives a very good impression of the response times seen in the samples: By scanning the beam, the defect could be relocated within 1.2 seconds from an initial position such that the initial defect vanished completely, and a new defect was induced and fully developed in the new position. Following these experiments at ambient temperature, the samples were heated to a temperature of 45 °C (Fig. 6) and the liquid crystal threshold behavior was studied in more detail. The samples were heated to a temperature of 45 °C, since this is a typical operation temperature, slightly higher than room temperature, not unusual for commercial LC mixtures (MLC-2087 has a clearing temperature of ≈100 °C). Exposure with various intensities showed, that formation of the umbilics could be already observed with exposure intensities as low as 0.36 mW, which was the minimum power required to see the effect. This corresponds to a power density of ≈150 Wcm^{-2} in the laser beam focus. It should be noted that the samples were exposed at normal incidence. For MLC 2087, the threshold intensity of the light induced optical Fredericks transition [41] (OFT) in a 30 µm thin sample is > 15 $kWcm^{-2}$. The minimum intensity required in the samples with a field generating Fe:LN substrate was therefore 2 orders of magnitude lower than would be expected for light induced director realignments in samples without Fe:LN substrates. Given the fringe fields generated by the substrates, this is not surprising, since the local realignment effect observed here was not due to the direct effect of light on LC molecules, but was induced by photovoltaic fields. At exposure intensities ≥ 0.36 mW, the fringe fields were high enough to realign the LC director such that the transmitted light intensity of the probe light was much higher than the detection limit of the camera (the detection limit of the camera used can present a detection threshold in alternative samples [41] with non-linear optical responses, which are intrinsically threshold free).

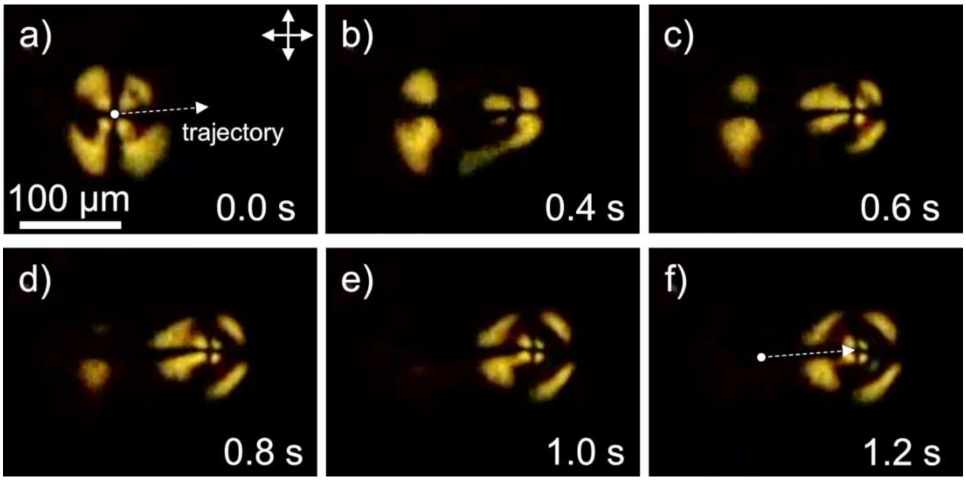

Fig. 5. Image sequence recorded upon relocation of exposure beam spot in MLC 2087. The orientation of the polarizers is indicated in (a) with double arrows.

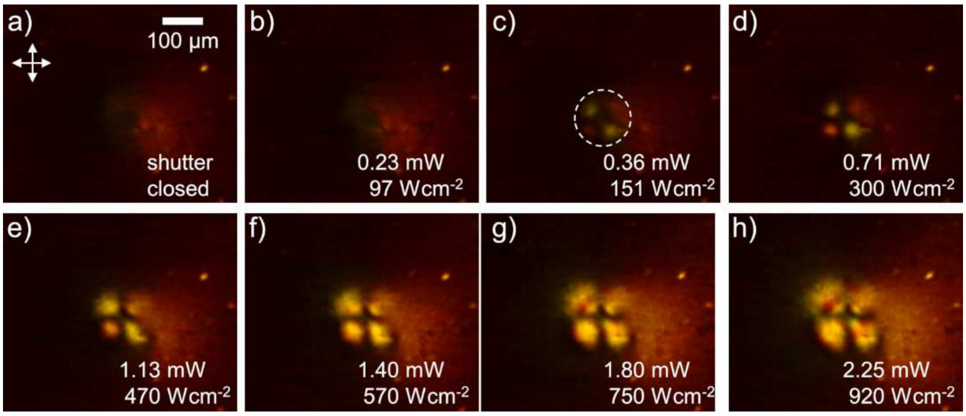

Fig. 6. Sample filled with MLC 2087 exposed at 45 °C with various exposure intensities. At an exposure intensity of 0.36 mW, LC realignment were already clearly seen. The orientation of the polarizers is indicated in (a) with double arrows.

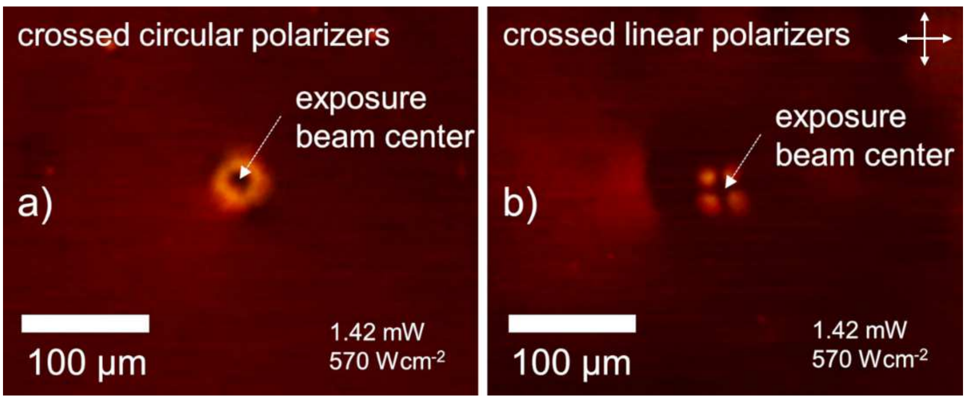

Fig. 7. Doughnut-shaped probe light beam generated in a sample filled with MLC 2087, exposed at 45 °C, and investigated with circularly polarized probe light and crossed, circular analyzer (second polarizer). (b) Pattern observed if the sample was investigated with linearly polarized probe light and crossed, linear analyzer. The orientation of these polarizers is indicated with double arrows.

Due to the presence of the field induced radial defect, the exposed samples are waveplates (q-plates) with the correct director distribution and two-dimensional optical phase profile to generate doughnut-shaped intensity profiles, if investigated between crossed circular polarizers. Such a doughnut-shaped intensity distribution is shown in Fig. 7a. The texture observed between crossed linear polarizers and under otherwise identical conditions is also shown in the Figure, for completeness. The diameter of the doughnut-shaped intensity distribution in Fig. 7a is $\approx$ 30 μm. The size can potentially be tuned by using exposure beam focusing lenses with various focal length and numerical apertures, which result in various exposure spot sizes.

2.2. LC with negative dielectric anisotropy

For reference, the same kind of cells were filled with MLC-6608, having negative dielectric anisotropy. Two different director reorientations were observed in this case. In contrast to the LC with positive dielectric anisotropy, the initial homeotropic orientation was not stabilized by the photovoltaic field at the exposure spot center in this LC. As shown in Fig. 8, exposure of the samples led to a different kind of director reorientation than in the experiments with MLC-2087: Although the director reorientation was still localized, the observed pattern was non-circular and did not have 4-fold symmetry. In contrast to the well-defined isogyres seen in the MLC-2087, the pattern seen in MLC-6608 showed birefringent stripes (highlighted with cyan colored lines in Fig. 8). The results observed in MLC-6608 indicate that both shape and size of the director realignment varied at various sample positions and – at least in the studied samples with a lecithin alignment layer - cannot be induced as reliably as in the MLC-2087 filled samples.

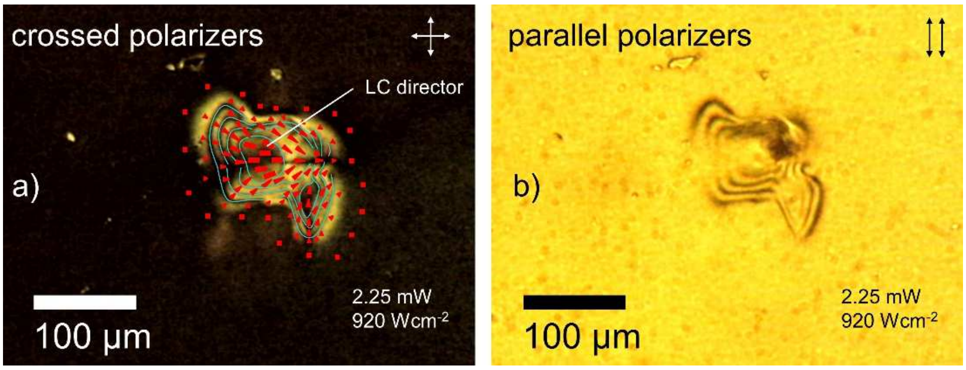

Fig. 8. Localized director reorientation recorded in MLC-6608 filled samples investigated with (a) crossed polarizers, (b) parallel polarizers. A schematic of the local director reorientation was placed in (a). Also, cyan colored lines were inserted as guide to the eye to highlight the dark, birefringent stripes. The orientation of the polarizers is indicated with double arrows.

3. Discussion

The isogyres and isochromes patterns seen in the MLC-2087 filled hybridized test cells were already a very good indication that the observed defects were actually umbilics. Anyway, the patterns observed between crossed circular polarizers can be further analyzed. Umbilics in liquid crystals with negative dielectric anisotropy were described by Rapini [1], with a very useful set of equations. As was shown in [5], this model can be applied to estimate the transmittance pattern of an umbilic defect between crossed circular polarizers. An umbilic can be described in polar coordinates, with φ representing the azimuth of the director and θ the local tilt angle (Fig. 1a). The local orientation of the LC director changes not only along the *z*-axis but along both the radial (*r*) and azimuthal (φ) polar coordinates at the same time [1]. The director field in a model umbilic can be expressed in Cartesian coordinates as:

$$n = \begin{pmatrix} n_x \\ n_y \\ n_z \end{pmatrix} = \begin{pmatrix} \sin\theta\cos\varphi \\ sin\theta sin\varphi \\ cos\theta \end{pmatrix}. \quad (1)$$

According to Rapini, model umbilics in a LC layer of thickness *d* can be described by considering 4 parameters. First, the symmetry of the umbilic is described with a set of two parameters: The topological strength, or charge, of the defect s ($s = \pm 1$), and a constant φ_0, which determines the shape of the director distribution in the *xy*-plane ($\varphi_0 = 0$ corresponds to radial alignment):

$$\varphi = s\varphi + \varphi_0. \quad (2)$$

The director tilt angle distribution is defined by the asymptotic value [5] θ_∞ of the director tilt angle at large *r*, and a reduced tilt amplitude $a\left(\frac{r}{r_{core}}\right)$ in the form $\theta(r,z) = \theta_\infty a\left(\frac{r}{r_{core}}\right)\sin\left(\frac{\pi z}{d}\right)$. In the present case, the electric field causing the defect formation is a divergent, localized field, not present all over the sample, but just in the irradiated region. Accordingly, there is no reorientation far away from the beam center. For this reason, one can use a modified expression for $\theta(r,z)$, taking into account a Gaussian envelope $\exp\left(-\frac{r^2}{w_1^2}\right)$ of the assumed charge distribution

$$\theta(r,z) = \theta_\infty a\left(\frac{r}{r_{core}}\right)\exp\left(-\frac{r^2}{w_1^2}\right)\sin\left(\frac{\pi z}{d}\right). \quad (3)$$

This model (Eq. 3) can be used to estimate the director profile in a localized, isolated umbilic defect. The equation results in $\theta(0,z) = 0$ and $\theta(r \gg r_{core}, z) = 0$. The local tilt angle is limited to a value considerably lower than θ_∞, if r_{core} and w_1 are of the same order of magnitude.

The transmittance can now be calculated. For light propagating along the z-direction, the local effective birefringence Δn_{eff} depends on the tilt angle distribution. The liquid crystal used, MLC-2087, has a low birefringence of Δn = 0.076. In the approximation $\Delta n << n$, where n is the average refractive index of a birefringent optical medium, the local effective birefringence can be calculated as [43,44]:

$$\Delta n_{eff}(r,z) = \Delta n \sin^2(\theta(r,z)). \quad (4)$$

The overall phase retardation acquired in the liquid crystal layer can then be estimated as:

$$\Gamma(\mathrm{r}) = \frac{2\pi}{\lambda}\int_0^d \Delta n_{eff}(r,z)dz = \frac{2\pi}{\lambda}\Delta n \int_0^d \sin^2(\theta(r,z))\, dz. \tag{5}$$

The integral in Eq. 5 is defined over the layer thickness of the LC layer. For imaging with crossed circular polarizers [5], the transcmittance can be obtained as:

$$T(r) = \frac{I_{out}^{\sigma\perp}(r)}{I_0} = \sin^2\left(\frac{\Gamma(\mathrm{r})}{2}\right), \tag{6}$$

where I_0 is the initial intensity and $I_{out}^{\sigma\perp}$ is the counter polarized output light field component. Accordingly, a radial transmission profile for a model umbilic observed between crossed circular polarizers can be obtained by inserting Eq. 3 in Eq. 5 and inserting the obtained result in Eq. (6):

$$T(r) = \sin^2\left(\Delta n \frac{\pi}{\lambda}\int_0^d \sin^2\left(\theta_\infty a\left(\frac{r}{r_{core}}\right)\exp\left(-\frac{r^2}{w_1^2}\right)\sin\left(\frac{\pi z}{d}\right)\right)dz\right). \tag{7}$$

The transmittance profile described by Eq. 7 has been numerically calculated in OriginPro. The characteristic line shape of the reduced tilt amplitude [1] was used and wavelength and layer thickness were set to 600 nm and 30 µm, respectively. The parameters θ_∞, w_1, and r_{core} were varied. The resulting profile line was compared to experimental data: The transmittance profile shown in Fig. 9a (black colored line with error markers) was extracted from a recorded pattern. As indicated in Fig. 9b, several radial profile lines were extracted and averaged, which resulted a profile line along with standard error.

As indicated in Figure 9a, the calculated model curve has been obtained by using $\theta_\infty = 1.23$, $w_1 = 20$ µm, and $r_{core} = 15.5$ µm. A sketch of the director profile obtained by inserting this set of parameters in Eq. 7 is shown in Fig. 9c. As seen in the figure, the director is parallel to the *z*-direction at the center of the defect ($r = 0$ µm) and in the area far away from the defect center ($r > 30$ µm), as expected in a localized, isolated umbilic. The local tilt angle is increasing in the range $0 < r < 12$ µm, where it reaches a maximum tilt angle of $\theta \approx 0.4$, and decreasing again at $r > 12$ µm. As expected, this relatively low reorientation (limited to θ < 0.4) locally already leads to high transmittance, due to the high layer thickness of 30 µm.

The model shown here is already a good qualitative description of the experimental results. The model curve shown in Fig. 9a almost fits the experimental data within the experimental error bar. Anyway, a quantitative description of the director realignment is still needed.

Some attempts were recently made [45] to predict the behavior of a LC in such samples by considering a field distribution with non-vanishing tangential field component near the ITO layer. However, the director field distribution shown in [45] had high tilt angles, which were monotonously increasing with increasing r, and exceeding a value of $\theta = 1$ at $r \approx 25$ µm. Accordingly, the simulation results shown in [45] did not result in homeotropic director alignment at $r >> r_{core}$ within the area of calculation.

It would be desirable if a theoretical model can predict the field induced reorientation in the investigated samples with isolated, localized umbilics in detail. Such a theoretical model should be capable to predict the coupling of exposure intensity and director reorientations, mediated by the photo generated fields, and should also be capable to describe the response times, the preferable thickness of substrates needed, the preferable doping concentration of Fe doped lithium niobate, predict desirable elastic properties of the LC and make it possible to select an alternative LC or give further directions for experimental work. Anyway, deriving such a model is beyond the scope of this experimental work.

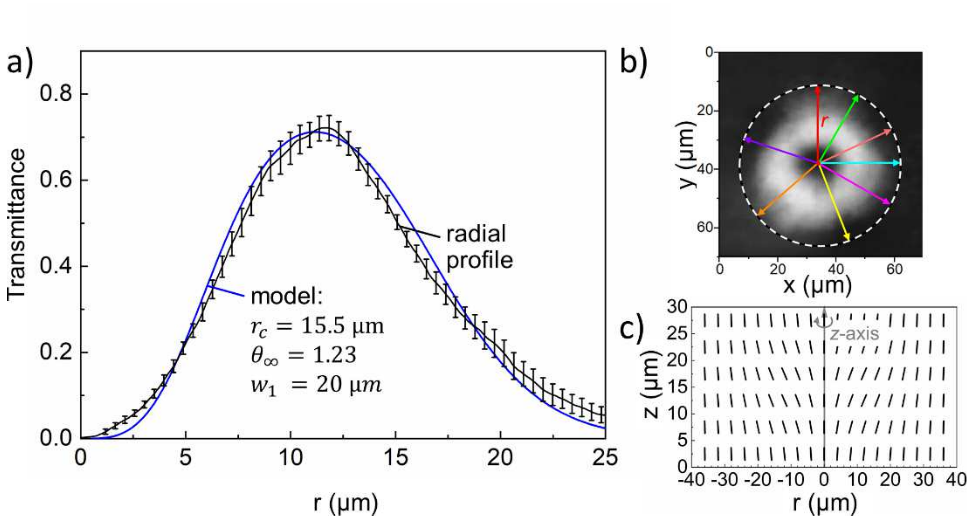

Fig. 9. (a) Radial transmission profile between crossed circular polarizers. An averaged profile line (black line) is shown (standard error indicated with error markers) and obtained for a model umbilic (parameters indicated in the figure). (b) Several radial scans were extracted from the recorded transmittance pattern and averaged. (c) Sketch of the director profile in the localized, isolated defect.

4. Conclusions

All optical formation of radial point defects (q-plates) in a LC with positive dielectric anisotropy is reported and the defects were identified as umbilics. The electric field leading to the formation of this kind of defect generated optically in hybridized LC cells made with a *z*-cut Fe:LN substrate and an ITO coated covering glass. There was no preferred orientation direction in the samples and both conditions, namely initial homeotropic alignment and no preferred orientation for reorientations in the *xy*-plane, for the formation of umbilic defects were fulfilled.

Localized exposure to a tightly focused Gaussian laser beam lead to appearance of umbilics with the typical isogyres and isochromes patterns (Fig. 3, Fig. 4), depending on the exposure optical power. A doughnut-shaped intensity profile was recorded by investigating the samples with crossed circular polarizers.

As shown, the spatial distribution of the photo-generated electric field in the samples had the correct circular symmetry and shape to fulfill the requirements to induce umbilical defects in the LC. The experimentally observed intensity distributions were compared to transmittance profiles expected for typical umbilics.

All optical formation of umbilics has also been tested in a liquid crystal with negative dielectric anisotropy. The approach still led to director reorientations, however, distorted defect patterns were obtained.

In contrast, the results obtained in the samples filled with the LC with positive dielectric anisotropy are promising for all optically controlled vortex generation. For example, the observed all optically generated umbilics can be easily relocated in the samples by scanning the laser beam to another position, as shown in Fig. 5, and potentially, patterns of umbilics can be induced at various positions by exposure with several laser beam spots.

The combination of soft matter and photoresponsive materials holds great promise in view of the realization of novel optical devices able to combine the peculiarity of the different components. Specifically, hybrid structures that mix lithium niobate and low molar mass nematic liquid crystals have recently been proposed as good candidates to be used in optofluidic devices. The possibility of using them to generate high quality umbilics through light irradiation, that was demonstrated here, is a further proof of the versatility of these combined systems and a step forward in the design of novel optofluidic devices with new functionalities.

5. Materials and Methods

Sample Preparation: Fe:LN substrates (z-cut, Fe-doping concentration 0.03 mol%, optical quality polished surfaces, 0.5 mm thickness, obtained from MTI Corporation) were cleaned by sonication in a water/surfactant dispersion, followed by cleansing and drying with acetone. Since the optic axis (c-axis in Fig. 2) was orthogonal to the sample plane in z-cut Fe:LN crystals, they appeared as would an optically isotropic medium in incident light at normal incidence (k-vector $\parallel z$) . Indium tin oxide (ITO) coated cover glasses were cleaned by the same process and additionally treated in a plasma cleaner for 1 minute. The cleaned substrates (Fe:LN substrates and ITO coated cover glasses) were coated with lecithin as anchoring agent to provide vertical (homeotropic) alignment of the LC director. Mylar film spacers were placed on the Fe:LN substrates and a cover glass was placed on top of these spacers with the ITO side facing towards the Fe:LN substrate. The cell gap was measured with a micrometer probe and a value of ≈ 30 μm was found. These empty samples were filled via capillary action by placing a droplet of LC at one sample edge and letting the LC flow in the gap between Fe:LN substrate and ITO-glass. When the test cells were filled completely, any excess was removed from the edges by using tissue (Kim wipes). Two LCs (obtained from Merck KGaA) were investigated. The LC MLC-2087 [34,36] had positive dielectric anisotropy ($\Delta\varepsilon = 13.31$), a birefringence of Δn = 0.076, and average elastic constant K = 14.7 pN. The second LC was MLC-6608 [42] with negative dielectric anisotropy $\Delta\varepsilon = -4.2$, birefringence Δn = 0.083, and an average elastic constant K ≈ 17 pN, comparable to that of the first LC. The clearing temperatures (phase transition from nematic to isotropic) of both LCs were ≈ 100 °C.

Exposure Setup: Samples were investigated and exposed in a modified inverted optical polarized microscope with a CMOS digital color camera with adjustable 10x zoom objective lens (TheImagingSource, DFK MKU120-10x22) and a coupled focused (lens with 10 cm focal width) diode laser beam (Thorlabs CPS 532) with a wavelength of 532 nm. A removable edgepass filter with a cut-on wavelength of 550 nm (Thorlabs FELH0550) could be inserted in the beam path of the microscope when needed. The birefringent patterns seen in the exposed samples were investigated with a collimated white light LED source (probe light). The focused exposure beam had a Gaussian intensity distribution in the sample plane with a full width at half maximum (FWHM) of 14.5 µm (investigated with a Spiricon SP620U beam profiler). The laser power was adjusted with neutral density filters and the samples were exposed with various exposure intensities for example a beam power of 1.43 mW (570 Wcm^{-2} power density in the sample plane) or a beam power of 2.25 mW (920 Wcm^{-2}).

Selected samples were investigated with circularly polarized probe light (crossed circular polarizers). If so, the linear polarized probe light source was fitted with an achromatic quarter-wave plate (oriented at an 45° angle) in order to generate circularly polarized probe light. The second polarizer of the microscope (analyzer), located between sample and camera, was then replaced with a circular film-polarizer.

Transmittance Profiles: The recorded images were converted to transmittance data by using OriginPro (Ver. 2019b, OriginLab Corporation): The images were converted to 16-bit (linear detector sensitivity) grayscale data. The extracted profile lines were background corrected to facilitate comparison to modelled data.

Acknowledgements

The authors are grateful to Prof. Pawel Pieranski (Laboratoire de Physique des Solides, Université Paris-Sud) and Prof. Victor Y. Reshetnyak (Department of Theoretical Physics, Taras Shevchenko National University of Kyiv) for fruitful discussions and critical reading. Dr. Samir Suweis (Department of Physics and Astronomy Galileo Galilei, University of Padova) and Dr. Raouf Barboza (Dipartimento SIMAU, Università Politecnica delle Marche, Ancona) are acknowledged for technical discussion of data evaluation. Ms. Atefeh Habibpourmoghadam (Paderborn University, Department of Chemistry) is thanked for fruitful discussions on optical vortex creation in liquid crystalline waveplates (q-plates), discussions on preliminary data, and discussions on the properties of umbilical defects.

Funded by the German Research Council (DFG) grant LO 1922/4-1 and by the US Air Force Office of Scientific Research (AFOSR) through the European Office of Aerospace Research & Development (EOARD) grant FA9550-18-1-7002.

References

[1] A. Rapini, Umbilics: static properties and shear-induced displacements, J. Phys. France. 34 (1973) 629–633. https://doi.org/10.1051/jphys:01973003407062900.

[2] E. Brasselet, Singular optical manipulation of birefringent elastic media using nonsingular beams, Opt. Lett. 34 (2009) 3229–3231. https://doi.org/10.1364/OL.34.003229.

[3] E. Brasselet, Spin-orbit optical cross-phase-modulation, Phys. Rev. A. 82 (2010). https://doi.org/10.1103/PhysRevA.82.063836.

[4] E. Brasselet, C. Loussert, Electrically controlled topological defects in liquid crystals as tunable spin-orbit encoders for photons, Opt. Lett. 36 (2011) 719–721. https://doi.org/10.1364/OL.36.000719.

[5] E. Brasselet, Tunable Optical Vortex Arrays from a Single Nematic Topological Defect, Phys. Rev. Lett. 108 (2012) 087801. https://doi.org/10.1103/PhysRevLett.108.087801.

[6] R. Barboza, U. Bortolozzo, M.G. Clerc, S. Residori, E. Vidal-Henriquez, Optical vortex induction via light-matter interaction in liquid-crystal media, Adv. Opt. Photon. 7 (2015) 635–683. https://doi.org/10.1364/AOP.7.000635.

[7] N. Kravets, E. Brasselet, Nonlinear unitary transformations of space-variant polarized light fields from self-induced geometric-phase optical elements, Phys. Rev. A. 97 (2018) 013834. https://doi.org/10.1103/PhysRevA.97.013834.

[8] N. Kravets, N. Podoliak, M. Kaczmarek, E. Brasselet, Self-induced liquid crystal q-plate by photoelectric interface activation, Appl. Phys. Lett. 114 (2019) 061101. https://doi.org/10.1063/1.5082598.

[9] R. Barboza, U. Bortolozzo, G. Assanto, S. Residori, Optical Vortex Generation in Nematic Liquid Crystal Light Valves, Mol. Cryst. Liq. Cryst. 572 (2013) 24–30. https://doi.org/10.1080/15421406.2012.763206.

[10] R. Barboza, U. Bortolozzo, G. Assanto, E. Vidal-Henriquez, M.G. Clerc, S. Residori, Harnessing Optical Vortex Lattices in Nematic Liquid Crystals, Phys. Rev. Lett. 111 (2013) 093902. https://doi.org/10.1103/PhysRevLett.111.093902.

[11] E. Brasselet, Tunable High-Resolution Macroscopic Self-Engineered Geometric Phase Optical Elements, Phys. Rev. Lett. 121 (2018) 033901. https://doi.org/10.1103/PhysRevLett.121.033901.

[12] P. Pieranski, B. Yang, L.-J. Burtz, A. Camu, F. Simonetti, Generation of umbilics by magnets and flows, Liquid Crystals. 40 (2013) 1593–1608. https://doi.org/10.1080/02678292.2012.742581.

[13] C. Loussert, K. Kushnir, E. Brasselet, Q-plates micro-arrays for parallel processing of the photon orbital angular momentum, Appl. Phys. Lett. 105 (2014) 121108. https://doi.org/10.1063/1.4895706.

[14] I.A. Budagovsky, A.S. Zolot'ko, M.P. Smayev, S.A. Shvetsov, Formation of the light beam with wavefront screw dislocation at the photorefractive effect in nematic liquid crystal, Bull. Lebedev Phys. Inst. 42 (2015) 319–322. https://doi.org/10.3103/S1068335615110032.
[15] I.A. Budagovsky, S.A. Shvetsov, A.S. Zolot'ko, Optical vortex generation in homeotropic NLCs in the presence of DC electric field, Mol. Cryst. Liq. Cryst. 637 (2016) 47–52. https://doi.org/10.1080/15421406.2016.1198663.
[16] R.B. Meyer, Point Disclinations at a Nematic-lsotropic Liquid Interface, Mol. Cryst. Liq. Cryst. 16 (1972) 355–369. https://doi.org/10.1080/15421407208082796.
[17] F. Simoni, Nonlinear Optical Properties of Liquid Crystals and Polymer Dispersed Liquid Crystals, WORLD SCIENTIFIC, 1997. https://doi.org/10.1142/2343.
[18] E. Brasselet, Singular optical reordering of liquid crystals using Gaussian beams, J. Opt. 12 (2010) 124005. https://doi.org/10.1088/2040-8978/12/12/124005.
[19] A. García-Cabañes, A. Blázquez-Castro, L. Arizmendi, F. Agulló-López, M. Carrascosa, Recent Achievements on Photovoltaic Optoelectronic Tweezers Based on Lithium Niobate, Crystals. 8 (2018) 65. https://doi.org/10.3390/cryst8020065.
[20] M. Carrascosa, A. García-Cabañes, M. Jubera, J.B. Ramiro, F. Agulló-López, $LiNbO_3$: A photovoltaic substrate for massive parallel manipulation and patterning of nano-objects, Appl. Phys. Rev. 2 (2015) 040605. https://doi.org/10.1063/1.4929374.
[21] C. Arregui, J.B. Ramiro, A. Alcázar, A. Méndez, J.F. Muñoz-Martínez, M. Carrascosa, Comparative theoretical analysis between parallel and perpendicular geometries for 2D particle patterning in photovoltaic ferroelectric substrates, J. Eur. Opt. Soc.-Rapid Publ. 10 (2015) 15026. https://doi.org/10.2971/jeos.2015.15026.
[22] J. Villarroel, H. Burgos, Á. García-Cabañes, M. Carrascosa, A. Blázquez-Castro, F. Agulló-López, Photovoltaic versus optical tweezers, Opt. Express. 19 (2011) 24320–24330. https://doi.org/10.1364/OE.19.024320.
[23] C. Arregui, J.B. Ramiro, Á. Alcázar, Á. Méndez, H. Burgos, Á. García-Cabañes, M. Carrascosa, Optoelectronic tweezers under arbitrary illumination patterns: theoretical simulations and comparison to experiment, Opt. Express. 22 (2014) 29099–29110. https://doi.org/10.1364/OE.22.029099.
[24] M. Gazzetto, G. Nava, A. Zaltron, I. Cristiani, C. Sada, P. Minzioni, Numerical and Experimental Study of Optoelectronic Trapping on Iron-Doped Lithium Niobate Substrate, Crystals. 6 (2016) 123. https://doi.org/10.3390/cryst6100123.
[25] B. Fan, F. Li, L. Chen, L. Shi, W. Yan, Y. Zhang, S. Li, X. Wang, X. Wang, H. Chen, Photovoltaic Manipulation of Water Microdroplets on a Hydrophobic $LiNbO_3$ Substrate, Phys. Rev. Applied. 7 (2017) 064010. https://doi.org/10.1103/PhysRevApplied.7.064010.
[26] S. Bonfadini, F. Ciciulla, L. Criante, A. Zaltron, F. Simoni, V. Reshetnyak, L. Lucchetti, Optofluidic platform using liquid crystals in lithium niobate microchannel, Sci. Rep. 9 (2019) 1062. https://doi.org/10.1038/s41598-018-37351-7.
[27] A. Lorenz, L. Jiao, D.R. Evans, Photovoltaic light valving induced in a vertically aligned nematic liquid crystal on a x-cut $Fe{:}LiNbO_3$ substrate, Opt. Data Process. Storage. 4 (2018) 8–13. https://doi.org/10.1515/odps-2018-0002.
[28] J.L. Carns, G. Cook, M.A. Saleh, S.V. Serak, N.V. Tabiryan, D.R. Evans, Self-activated liquid-crystal cells with photovoltaic substrates, Opt. Lett. 31 (2006) 993–995. https://doi.org/10.1364/OL.31.000993.
[29] J.L. Carns, G. Cook, M.A. Saleh, S.V. Serak, N.V. Tabiryan, S.A. Basun, D.R. Evans, Photovoltaic Field-Induced Self-Phase Modulation of Light in Liquid Crystal Cells, Mol. Cryst. Liq. Cryst. 453 (2006) 83–92. https://doi.org/10.1080/15421400600651757.
[30] L. Lucchetti, K. Kushnir, A. Zaltron, F. Simoni, Light controlled phase shifter for optofluidics, Opt. Lett. 41 (2016) 333–335. https://doi.org/10.1364/OL.41.000333.

[31] L. Lucchetti, K. Kushnir, A. Zaltron, F. Simoni, Liquid crystal cells based on photovoltaic substrates, J. Eur. Opt. Soc.-Rapid Publ. 11 (2016) 16007. https://doi.org/10.2971/jeos.2016.16007.
[32] L. Lucchetti, K. Kushnir, V. Reshetnyak, F. Ciciulla, A. Zaltron, C. Sada, F. Simoni, Light-induced electric field generated by photovoltaic substrates investigated through liquid crystal reorientation, Opt. Mater. 73 (2017) 64–69. https://doi.org/10.1016/j.optmat.2017.08.004.
[33] L. Lucchetti, K. Kushnir, F. Ciciulla, A. Zaltron, G. Bettella, G. Pozza, C. Sada, V. Reshetnyak, F. Simoni, All-optical phase shifter with photovoltaic liquid crystal cell, in: Liquid Crystals XX, Proc. SPIE, 2016: p. 99400G. https://doi.org/10.1117/12.2235580.
[34] A. Habibpourmoghadam, L. Lucchetti, D.R. Evans, V.Y. Reshetnyak, F. Omairat, S.L. Schafforz, A. Lorenz, Laser-induced erasable patterns in a N* liquid crystal on an iron doped lithium niobate surface, Opt. Express. 25 (2017) 26148–26159. https://doi.org/10.1364/OE.25.026148.
[35] A. Habibpourmoghadam, L. Jiao, F. Omairat, D.R. Evans, L. Lucchetti, V. Reshetnyak, A. Lorenz, Confined photovoltaic fields in a photo-responsive liquid crystal test cell, in: Liquid Crystals XXI, Proc. SPIE, 2017: p. 1036112. https://doi.org/10.1117/12.2273990.
[36] A. Habibpourmoghadam, L. Jiao, V. Reshetnyak, D.R. Evans, A. Lorenz, Optical manipulation and defect creation in a liquid crystal on a photoresponsive surface, Phys. Rev. E. 96 (2017) 022701. https://doi.org/10.1103/PhysRevE.96.022701.
[37] S.L. Schafforz, Y. Yang, A. Lorenz, Defect formation in N* LCs via photovoltaic fields: impact of surface treatment, Liq. Cryst. 46 (2019) 2013–2022. https://doi.org/10.1080/02678292.2019.1626923.
[38] E.M. Purcell, D.J. Morin, Electricity and magnetism, Third edition, Cambridge University Press, Cambridge, 2013.
[39] A. Aleksanyan, N. Kravets, E. Brasselet, Multiple-Star System Adaptive Vortex Coronagraphy Using a Liquid Crystal Light Valve, Phys. Rev. Lett. 118 (2017) 203902. https://doi.org/10.1103/PhysRevLett.118.203902.
[40] L. Marrucci, Generation of Helical Modes of Light by Spin-to-Orbital Angular Momentum Conversion in Inhomogeneous Liquid Crystals, Mol. Cryst. Liq. Cryst. 488 (2008) 148–162. https://doi.org/10.1080/15421400802240524.
[41] N.V. Tabiryan, A.V. Sukhov, B.Y. Zel'dovich, Orientational Optical Nonlinearity of Liquid Crystals, Mol. Cryst. Liq. Cryst. 136 (1986) 1–139. https://doi.org/10.1080/00268948608074569.
[42] D. Cuypers, Vertically Aligned Nematic Liquid Crystal Microdisplays for Projection Applications, Ghent University, 2005. Data in Appendix B. http://hdl.handle.net/1854/LU-470265 (accessed January 20, 2020).
[43] R. A. Soref, M. J. Rafuse, Electrically Controlled Birefringence of Thin Nematic Films, J. Appl. Phys. 43 (1972), 2029–2037. https://doi.org/10.1063/1.1661449.
[44] M. Born, E. Wolf, Principles of Optics: Electromagnetic Theory of Propagation, Interference and Diffraction of Light, 6th ed.; Pergamon Press: Oxford ; New York, 1980.
[45] A. Habibpourmoghadam, Theoretical prediction of umbilics creation in nematic liquid crystals with positive dielectric anisotropy, ACS Omega 4 (2019) 21459–21468. https://doi.org/10.1021/acsomega.9b03158.

Highlights

- Relocatable umbilic defects in a liquid crystal with positive dielectric anisotropy
- Defects act as q-plates
- Test cells with Fe:$LiNbO_3$ substrate and indium tin oxide covering glass
- Samples driven with photovoltaic fields
- All optically generated effect

Graphical Abstract

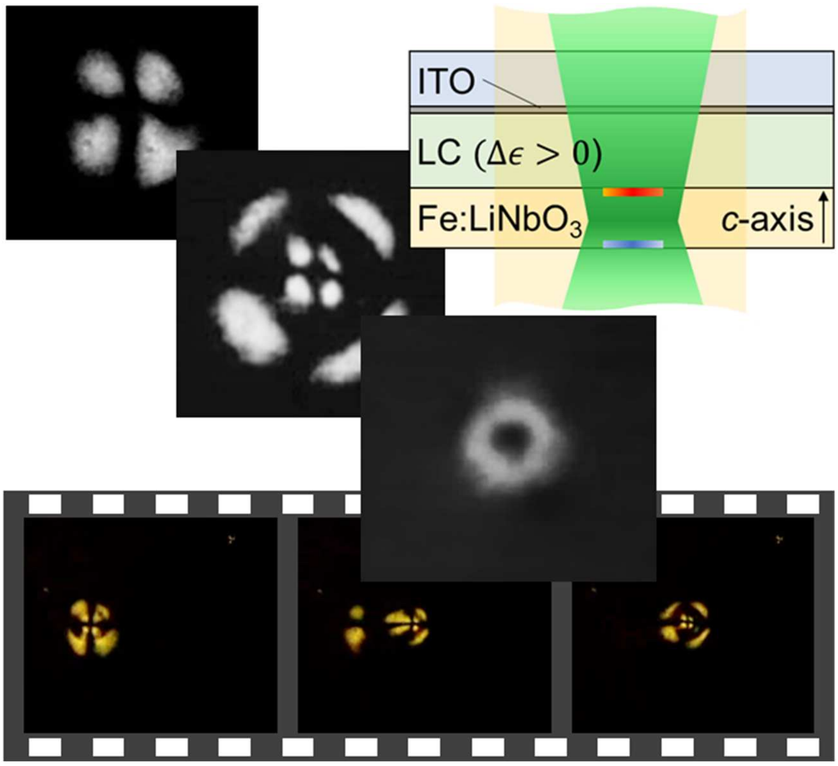

Graphical Abstract.

Figures

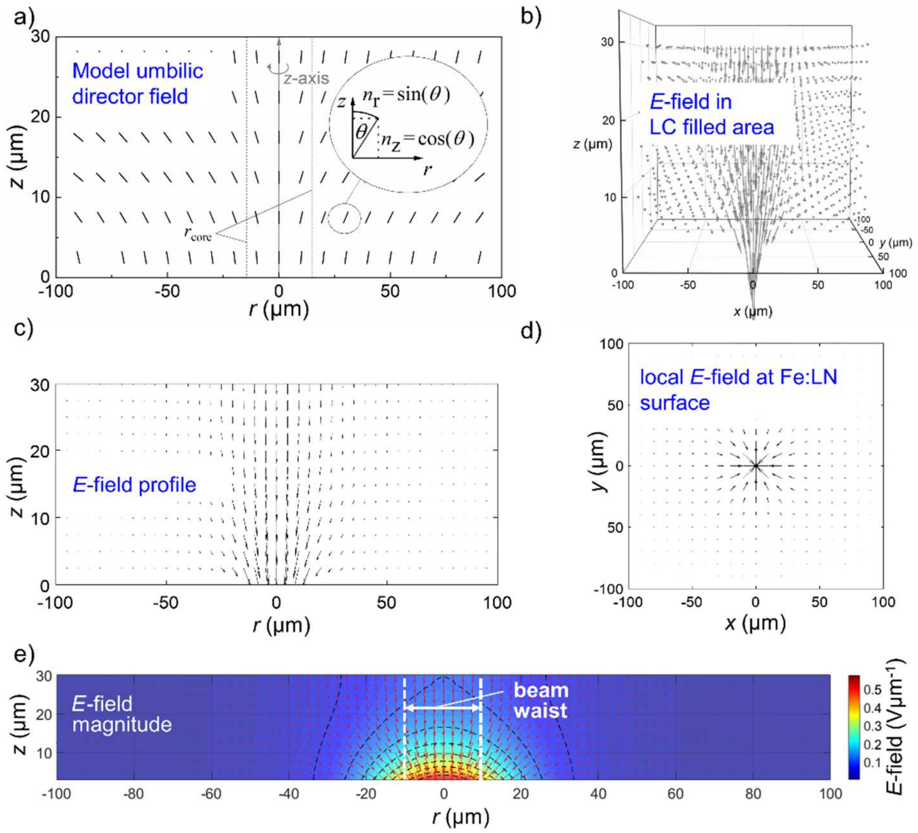

Fig. 1. (a) Director field in a model umbilic. (b) Three-dimensional electric field distribution expected in a sample driven with photovoltaic fields. A value of $\epsilon_{iso} = 7.3$ was used in the LC filled region to calculate the local field distribution. The field distribution was obtained by placing charge distributions on the surfaces of the Fe:LN crystal and applying the image charge method. (c) Profile view of the electric field distribution. (d) Aerial view of the local field distribution at the Fe:LN surface. (e) Magnitude of the field distribution in profile view.

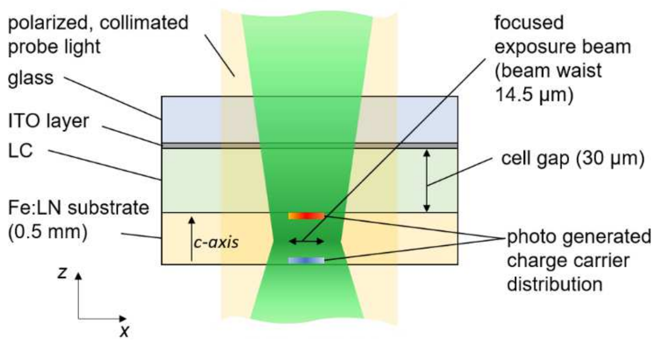

Fig. 2. Schematic of exposed hybridized LC test cell. The samples were investigated with collimated, polarized probe light.

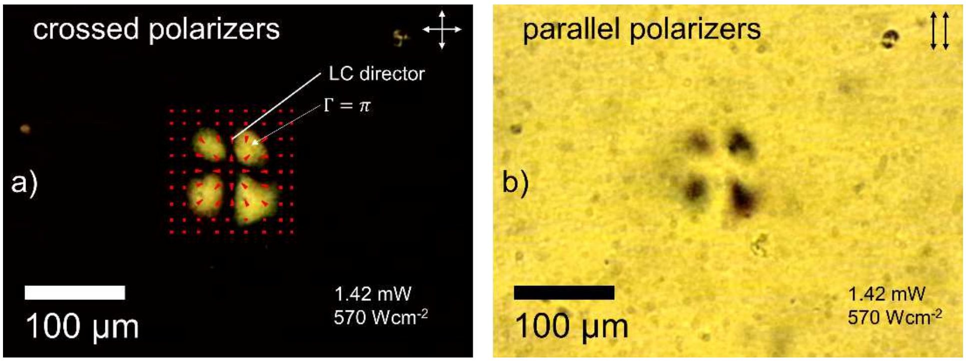

Fig. 3. Polarized optical micrographs of a sample filled with MLC 2087 exposed to a diode laser beam of 1.42 mW overall optical power. The sample was investigated with (a) crossed polarizers, (b) parallel polarizers. A schematic of the LC alignment in and near the locally induced defect was placed in (a). The orientation of the polarizers is indicated with double arrows.

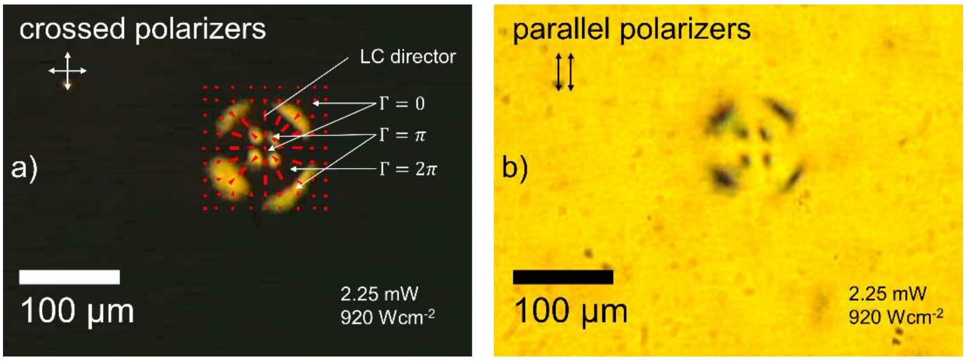

Fig. 4. Polarized optical micrographs of a sample filled with MLC 2087 exposed to a diode laser beam of 2.25 mW overall optical power. The sample was investigated with (a) crossed polarizers, (b) parallel polarizers. A schematic of the LC alignment in and near the locally induced defect was placed in (a). The orientation of the polarizers is indicated with double arrows.

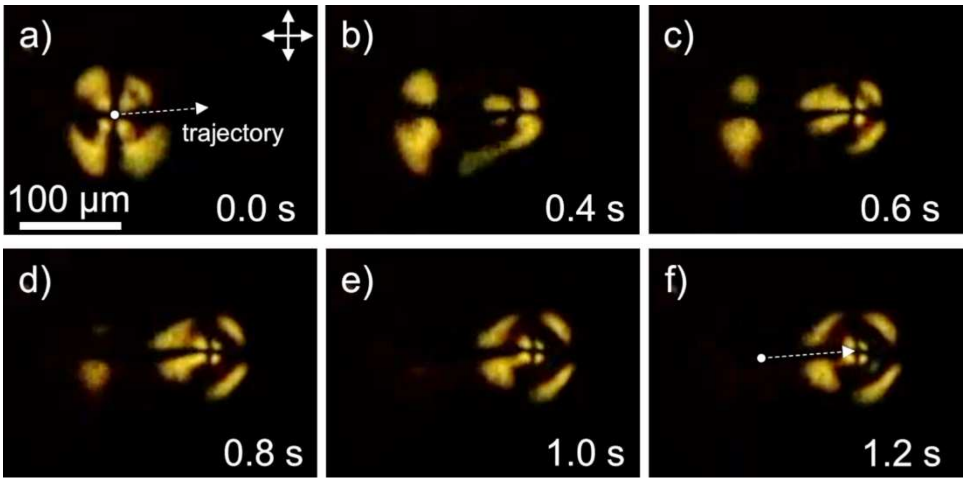

Fig. 5. Image sequence recorded upon relocation of exposure beam spot in MLC 2087. The orientation of the polarizers is indicated in (a) with double arrows.

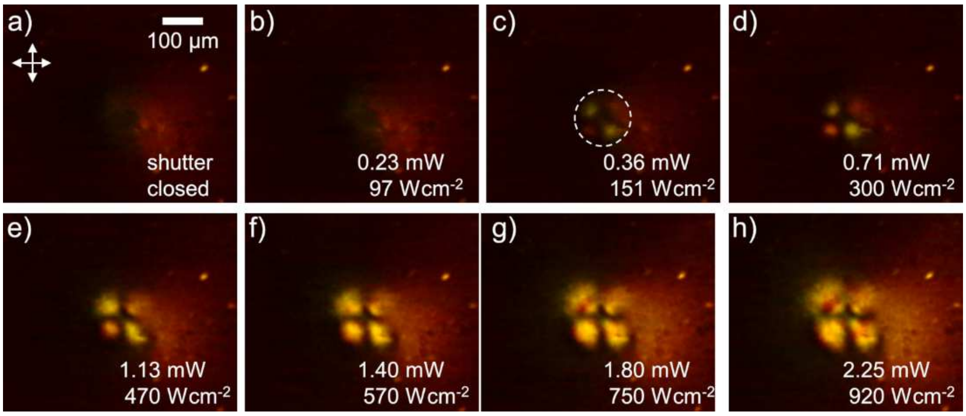

Fig. 6. Sample filled with MLC 2087 exposed at 45 °C with various exposure intensities. At an exposure intensity of 0.36 mW, LC realignment were already clearly seen. The orientation of the polarizers is indicated in (a) with double arrows.

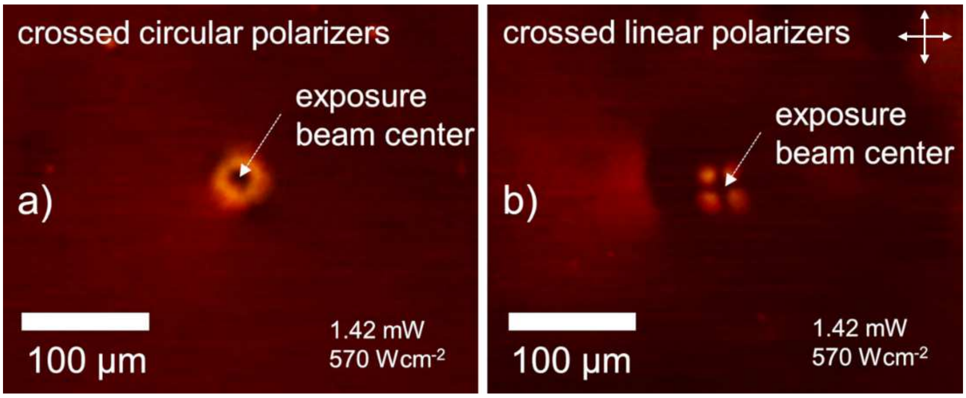

Fig. 7. Doughnut-shaped probe light beam generated in a sample filled with MLC 2087, exposed at 45 °C, and investigated with circularly polarized probe light and crossed, circular analyzer (second polarizer). (b) Pattern observed if the sample was investigated with linearly polarized probe light and crossed, linear analyzer. The orientation of these polarizers is indicated with double arrows.

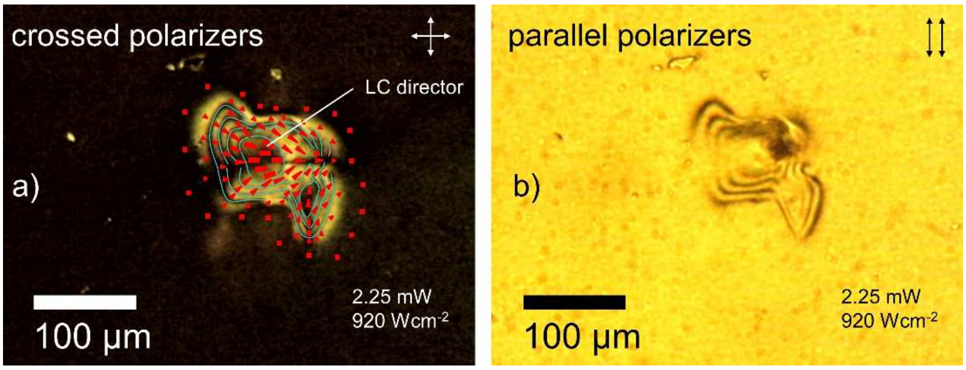

Fig. 8. Localized director reorientation recorded in MLC-6608 filled samples investigated with (a) crossed polarizers, (b) parallel polarizers. A schematic of the local director reorientation was placed in (a). Also, cyan colored lines were inserted as guide to the eye to highlight the dark, birefringent stripes. The orientation of the polarizers is indicated with double arrows.

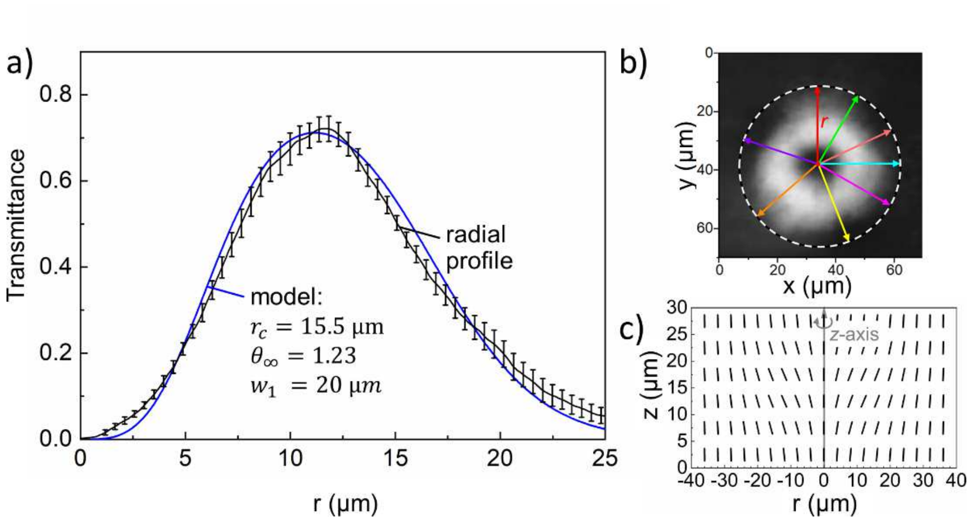

Fig. 9. (a) Radial transmission profile between crossed circular polarizers. An averaged profile line (black line) is shown (standard error indicated with error markers) and obtained for a model umbilic (parameters indicated in the figure). (b) Several radial scans were extracted from the recorded transmittance pattern and averaged. (c) Sketch of the director profile in the localized, isolated defect.

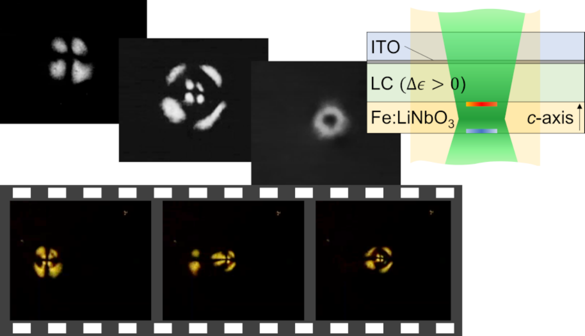
ITO
LC ($\Delta\epsilon > 0$)
Fe:LiNbO$_3$
c-axis